IEEE Photonics Journal
An IEEE Photonics Society Publication

Open Access

Experimental Study of a Multispectral Piston Sensing Technology

Volume 11, Number 3, June 2019

Li Dong
Haotong Ma
Qi Peng
Ge Ren
Bo Qi
Shanchao Liu
Zongliang Xie

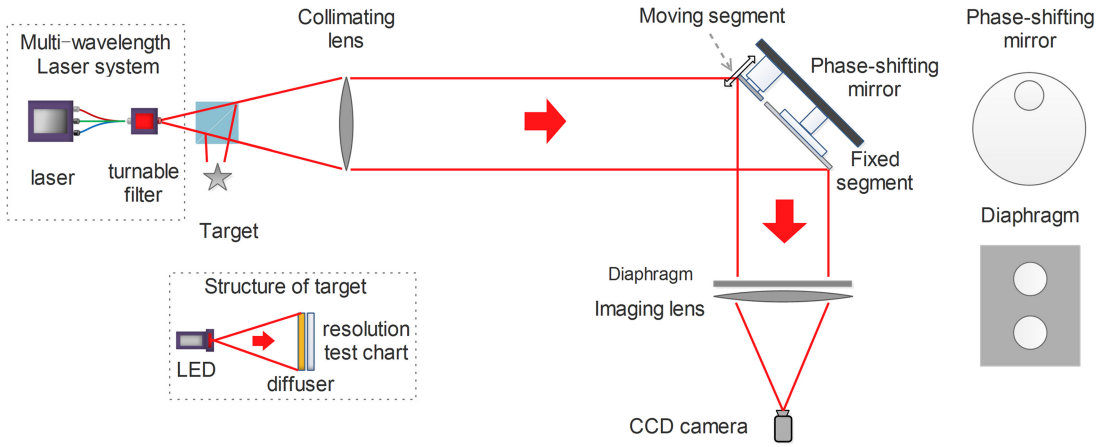

DOI: 10.1109/JPHOT.2019.2915018
1943-0655

Experimental Study of a Multispectral Piston Sensing Technology

Li Dong [1,2,3] **Haotong Ma** [1,2] **Qi Peng,** [1,2] **Ge Ren,** [1,2] **Bo Qi** [1,2] **Shanchao Liu,** [1,2,3] **and Zongliang Xie** [1,2,3]

[1]Key Laboratory of Optical Engineering, Chinese Academy of Sciences, Chengdu 610209, China
[2]Institute of Optics and Electronics, Chinese Academy of Science, Chengdu 610209, China
[3]University of Chinese Academy of Science, Beijing 100039, China

DOI:10.1109/JPHOT.2019.2915018

Manuscript received January 13, 2019; revised April 29, 2019; accepted April 30, 2019. Date of publication May 6, 2019; date of current version May 16, 2019. This work was supported by the National Natural Science Foundation of China under Grants 61775239 and 61205144. Corresponding authors: Li Dong and Haotong Ma (e-mail: wulfiyee@163.com; mahaotong@163.com).

Abstract: Nowadays giant segmented telescopes and multiaperture telescopes have grown out of the quest for high-resolution observations in astronomy. One of the major issues is the phasing of such telescopes. A concept of multispectral piston sensing technology is, therefore, re-examined and studied experimentally for the first time. Based on the phase-shifting "Telescope-Interferometer" technology and multispectral information, the multispectral piston sensing technology was assumed to be feasible with the segmented telescopes and multiaperture telescopes. In this paper, the optical scheme for this method has been designed and realized. Experimental tests have been carried out and demonstrated that the method is effective for piston sensing in a large capture range with high-precision despite some instrument-related limitations that can be eliminated. In our tests, the shortest coherent length of the three working spectrums we chose was less than 17.5 μm. Results show that the method successfully handled an amplitude of correction of about ± 8 μm with an accuracy of about $\lambda/30$ ($\lambda = 535$ nm) RMS in our tests, and we can foresee that the capture range can be enlarged if we choose working spectrums with larger coherent lengths.

Index Terms: Phase measurement, phased-array imaging systems, phase shift, imaging systems.

1. Introduction

To achieve fainter and further astronomical observations, there is increasingly continuous demand for higher angular resolution and better light collecting efficiency. Hence, both ground-based and space-based telescopes are heading in the direction of larger apertures. However, due to the restriction of current manufacturing technology, monolithic mirror telescopes are nearing their limits on size and weight [1], [2]. In contrast, multi-aperture telescopes or segmented telescopes don't have those limitations. Since the building of 10 m segmented telescope Keck [3], [4] in 1991 at Hawaii, many segmented systems have been built or are under construction, such as the El Gran Telescopio de Canarias (GTC) [5] with a 10.4 m diameter and 36 segments at La Palma Island, the James Webb Space Telescope (JWST) [6] with a 6.5 m diameter and 18 segments deployable primary mirror, the Thirty Meter Telescope (TMT) [7] with a 30 m diameter and 492 segments, and the European Extremely Large Telescope (E-ELT) [8] with a 39 m diameter and 798 segments in Paranal. In a segmented telescope, the primary mirror is created by splicing an array of actuated

hexagonal segmented mirrors together, which makes it easier to fabricate than the monolithic mirror of equivalent size in a monolithic mirror telescope. Multi-aperture telescopes have also been widely studied, including the Large Binocular Telescope (LBT) [9], Adaptive Reconnaissance Golay-3 Optical Satellite (ARGOS) [10], and Star-9 [11]. In a multi-aperture system, an array of afocal telescopes is combined to achieve a resolution equivalent to the resolution of a primary mirror with the entire array size.

For both the giant segmented and multi-aperture telescopes, it is required that the individual images from the segments or sub apertures are superposed coherently so as to achieve high resolution. Thus, the optical path differences (OPD) between the segment mirrors or sub-apertures must be measured accurately and calibrated to very tight tolerances in real time, which is the "co-phasing" process of telescopes. A lot of co-phasing methods have been developed. Both modified Shack-Hartman sensor and curvature sensor have been applied on segmented telescopes [12], [13]. However, these sensors often require special hardware such as actuated elements and additional optics, which will introduce non-common path errors. Phase diversity technology and its derivative methods have been used to detect the phase aberrations in multi-aperture imaging systems [1], [2], [14]–[16]. Nevertheless, these techniques often need significant post-processing times for the complex computations, which prevent their applications in real-time systems. The dispersed speckle (DS) method, which consists in generating a cube of spectrally dispersed images, can be applied to an arbitrary number of apertures in any geometrical configuration, but this method also needs a long processing time [17]. In contrast, a multi spectral piston sensing technology developed by François Hénault [18] has been shown to be able to measure the co-phasing errors fast and directly with simple numerical calculation in both segmented mirrors and multi-aperture telescope systems. Compared to the modefied Shack-Hartman sensor and curvature sensor, the hardware requirements are more moderate in this method. In addition, the multi spectral piston sensing technology can ensure the accuracy of measurement in a wide capture range.

In this paper, we choose to re-examine the multi spectral piston sensing technology. The multi spectral piston sensing technology evaluated in this paper is first described in monochromatic case by François Hénault in reference [19] as a conceptual design of a phase-shifting telescope-interferometer before being extending to multi-wavelength case. Based on an instrument we designed, we present the experimental demonstration of the multi spectral piston sensing technology in this paper. The accuracy and practical available measurement range of the technology are also evaluated.

This paper is organized as follows. We first briefly review the theory of the multi spectral piston sensing technology. Then, we characterize the optical scheme for experimental evaluation, and also design and make a phase-shifting instrument for the multi spectral piston sensing technology. Then, the experimental results are presented and the accuracy and measurement range of the technology are discussed in detail. Finally, conclusions and possible future advances are given.

2. Theory

In this section, multi spectral piston sensing technology is briefly introduced, while the detailed description can be found in ref [18]. By combining the main pupil of a telescope with a reference pupil, modulated and phase-shifted point spread functions for a specific wavelength can be generated. The fractional piston error can be extracted from demodulating the Fourier transforms of the point spread functions (PSFs). However, the estimation of the piston error is problematic due to the existence of the so-called "2π ambiguity". To resolve this ambiguity, different piston errors within 2π were derived from different phase-shifted PSFs at a few discrete wavelengths. The combination of multiple spectral measurement results allows the piston term to be recovered with high accuracy even in the presence of large piston errors.

Here, taking a golay-3 sparse aperture telescope as an example, the mathematical description of the multi-spectral piston sensing technology is given. As shown in Fig. 1(a), the three sub-apertures are circular and have the same diameter, while a reference pupil is configurated in the middle of the golay-3 pupil plane. It is noteworthy that the reference pupil can be located at other places

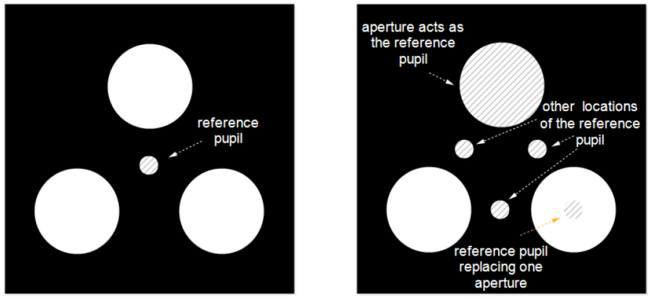

Fig. 1. Pupil configurations: (a) the golay-3 apertures with a reference pupil, (b) possible locations of the reference pupil.

of the pupil plane, or even replace one of the three sub-apertures. Fig. 1(b) shows other possible locations of the reference pupil.

If the pupil plane coordinates (u, v) and a phase-shift φ_m to the central reference pupil is introduced, the complex amplitude $A_m(u, v)$ in the exit plane (u, v) can be written as:

$$A_m(u, v) = P(u, v)e^{2i\pi\delta(u,v)/\lambda} + P_r(u, v)e^{j\varphi_m} \tag{1}$$

where m ranges from 1 to M, representing that φ_m will further take M different values; P(u, v) is the amplitude of the golay-3 pupil plane; $\delta(u, v)$ is the piston function; λ is the operation wavelength; $P_r(u, v)$ is the amplitude transmitted by the reference pupil.

In the case of a point light source, the complex amplitude in the telescope image plane at (x, y) is equal to the Fourier transform of $A_m(u, v)$. The Point Spread Function $PSF_m(x, y)$ of the imaging system is equal to the square modulus of the complex amplitude by definition. Also $PSF_m(x, y)$ can be easily acquired by the detector arranged in the image plane:

$$PSF_m(x, y) = \left|FT\left[A_m(u, v)\right]\right|^2 \tag{2}$$

where FT represents the Fourier transform operation.

The associated Optical Transfer Function (OTF) can be derived:

$$OTF_{\varphi_m} = FT^{-1}\left[PSF_m(x, y)\right] \tag{3}$$

If the values $\{0, \pi/2, \pi, 3\pi/2\}$ of the phase shift φ_m were given, the corresponding OTFs, i.e.,$\{OTF_0, OTF_{\pi/2}, OTF_\pi, OTF_{3\pi/2}\}$, can be calculated. Combining all these OTFs linearly and the result C can be calculated as follows:

$$\begin{aligned} C &= \frac{1}{M}\sum_{m=1}^{M} OTF_{\varphi_m}e^{j\varphi_m} \\ &= e^{\frac{2i\pi\delta(u,v)}{\lambda}}P(u, v) \otimes P_r(u, v) \\ &\quad + \frac{1}{4}(e^0 + e^{j\pi/2} + e^{j\pi} + e^{3i\pi/2})(OTF + OTF_r) \\ &\quad + \frac{1}{4}(e^0 + e^{j\pi} + e^{2i\pi} + e^{3i\pi})e^{-2i\pi\delta(-u,-v)/\lambda}P(-u, -v) \otimes P_r(u, v) \end{aligned} \tag{4}$$

where OFT represents the Optical Transfer Function of the Golay-3 pupil plane, OTF_r represents the Optical Transfer Function of the reference pupil and $\otimes$ operator represents convolution. Since the last two terms in Eq. (4) are equal to zero, the first term can be easily isolated from the others. Assuming the term $P_r(u, v)$ can be replaced with the Dirac distribution, the convolution product can

then be neglected. Consequently, we can get:

$$e^{\frac{2i\pi\delta(u,v)}{\lambda}} P(u,v) \approx \frac{1}{4}\left(OTF_0 + iOTF_{\pi/2} - OTF_\pi - iOTF_{3\pi/2}\right) \tag{5}$$

Then the decimal part of $\delta(u, v)$ after removing the integer multiple of 2π, which is defined as the fractional phase, can be extracted:

$$\phi_\lambda = \frac{1}{2\pi}\arctan\frac{\mathrm{Im}(OTF_0 + iOTF_{\pi/2} - OTF_\pi - iOTF_{3\pi/2})}{\mathrm{Re}(OTF_0 + iOTF_{\pi/2} - OTF_\pi - iOTF_{3\pi/2})} \tag{6}$$

where Re( ) and Im( ) respectively stand for the real part and imaginary part of a complex number, arctan represents the inverse tangent function. The value of the fractional phase ϕ_λ is within π and can be extended to a range of 2π when we take into consideration the positive or negative nature of the real part and the imaginary part.

In the first step of the multi-spectral piston error sensing technology, we need to acquire three groups of PSF images at three wavelengths, i.e., $\{\lambda_1, \lambda_2, \lambda_3\}$ and calculate the corresponding fractional phase errors $\{\phi_{\lambda_1}, \phi_{\lambda_2}, \phi_{\lambda_3}\}$. Since these fractional errors are within 2π, the second step is to extend the measurement range and figure out the complete Optical Path Differences (OPD) $\delta(u, v)$ via combining the phase shift measurements obtained at three different wavelengths. The sought piston $\delta(u, v)$ can be determined by resolving:

$$\delta(u,v) = (n_1 + \phi_1)\lambda_1 = (n_2 + \phi_2)\lambda_2 = (n_3 + \phi_3)\lambda_3 \tag{7}$$

where n1, n2 and n3 are positive or negative integers. This under-constrained system can be solved by using a simple unwrapping procedure over a limited capture range $[-\lambda_s/2,\ \lambda_s/2]$, where $\lambda_s = [\frac{1}{\lambda_1} - \frac{2}{\lambda_2} + \frac{1}{\lambda_3}]^{-1}$ is defined as the "synthetic wavelength". Firstly, guessing the piston error as:

$$\delta_0 = \lambda_s(\phi_1 - 2\phi 2 + \phi_3) - \lambda_s NINT(\lambda_s(\phi_1 - 2\phi 2 + \phi_3)/\lambda_s) \tag{8}$$

where NINT means taking the nearest integer of a number. Then the sought piston $\delta(u, v)$ can be calculated:

$$\delta(u,v) = \frac{1}{3}\sum_{k=1}^{3}\lambda_k(NINT(\delta_0/\lambda_k - \phi_k) + \phi_k) \tag{9}$$

3. Description of the Experimental Scheme

In order to test the performance of the multi-spectral piston sensing technology, it was applied to measure the co-phasing error of the sub-apertures in a sparse imaging system. Before the presentation of the optical setup, the phase-shifting instrument is introduced first.

3.1 Phase-Shifter

As has been pointed out in the former section, accurate and successive phase-shifts on the reference pupil are essential for the technology. Thus, a phase-shifter was designed for the experiment. As illustrated in Figs. 2 and 3, the phase-shifter is mainly composed of two segments, of which one can move and the other one is fixed. The inner circular moving segment is driven by a nanopositioning stage (Sanying MotionControl's product: NS152032), which enables the circular mirror to move slightly along the arrow direction. The closed loop control accuracy of the nanopositioning stage is 3 nm. Therefore, the collimated light illuminated on the moving segment can be modified with an accurate phase-shift φ_m before being reflected. The outer annular mirror is fixed on the metal plate so that the collimated light is reflected without phase modulation. The position and direction of the metal plate can be roughly adjusted by manually rotating the four screws arranged in the back of the metal plate. The implementation of the phase-shifter is shown in Fig. 2(b) and (c).

The angle between the collimated beam and the reflecting surfaces of the phase-shifter is $\pi/4$. When the inner circular segment moves a distance of h, the optical path of the beam reflected

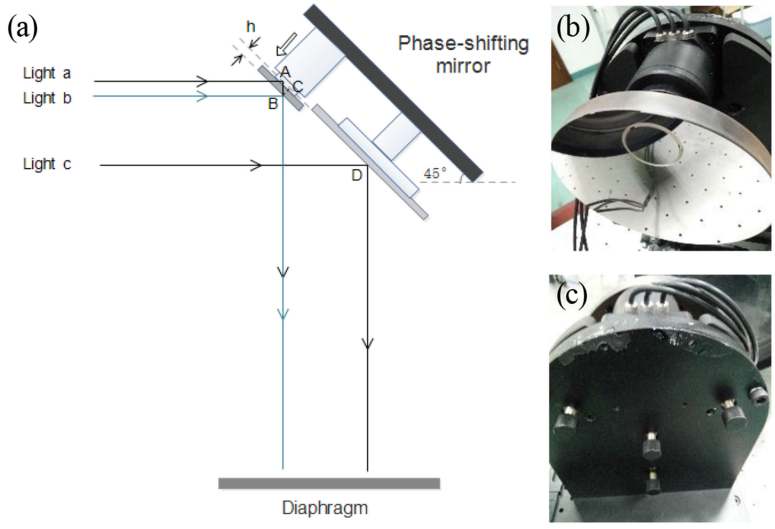

Fig. 2. The schematic diagram and the implementation of the phase-shifter, (a) the schematic diagram of the phase-shifter, (b) the front of the phase-shifter implementation, (c) the back of the phase-shifter implementation.

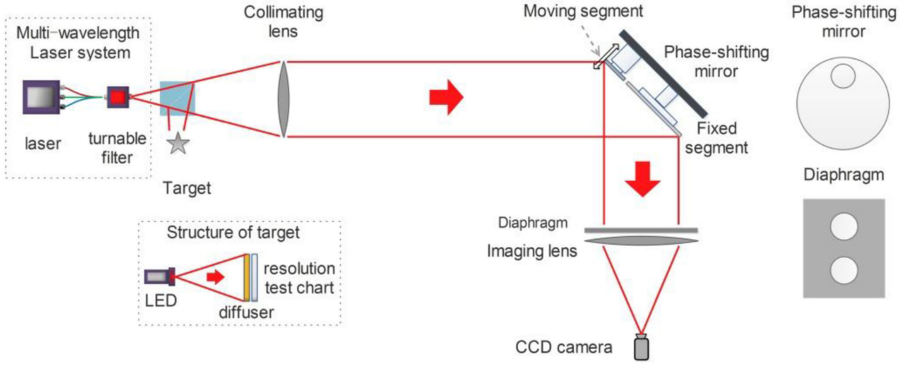

Fig. 3. The configuration of the optical setup.

by the circular segment changes $\sqrt{2}h$.The relation can be easily obtained from the three rays of light (light a, light b and light c) in Fig. 3(a), which leads to the expression of the corresponding phase-shift φ_m:

$$\varphi_m = 2\sqrt{2}\pi nh/\lambda \tag{10}$$

where λ is the operation wavelength, n represents the refractive index and its value is 1 as the beams travels in the air. From the above equation, the displacement of the moving segment can be extracted for modifying the collimated light with a specific phase-shift.

3.2 Description of the Optical Setup

The experimental setup is shown in Fig. 3 and the implementation of the experimental optical setup is shown in Fig. 4. A diaphragm with two identical apertures which are vertically arranged is used to simulate the two-aperture telescopes for simplicity with the upper aperture as the reference pupil. A collimator with a focal length of 3000 mm is used here as a scene projector.

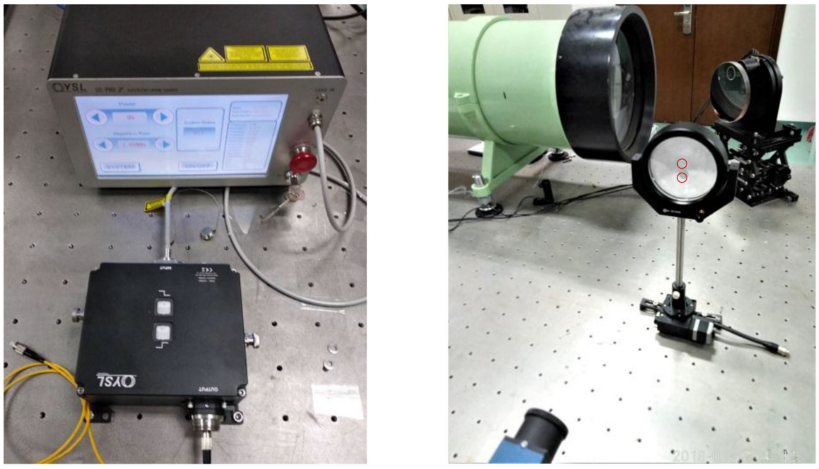

(a) (b)

Fig. 4. The implementation of the experimental optical setup, (a) the light source consists of a super-continuum fiber laser and a tunable filter system, (b) implementation of the experimental optical setup, a large collimator collimates the beam from the light source before the beam travels to the phase-shifter.

A multi-spectral point source is used as the scene to calibrate the optical scheme and co-phase the two-aperture telescopes. The point source is a supercontinuum fiber laser (Yangtze Soton Laser's product: SC-Pro 7). The supercontinuum source is equipped with a tunable filter system (Yangtze Soton Laser's product: VLF3580), thus several narrow spectrums of different central wavelength can be obtained. The divergent beam which comes from the point source is collimated by the collimator and then travels towards the phase-shifter. The two segments of the phase-shifter divide the collimated beam into two paths and reflect them to the two-aperture telescope. The beam from the moving segment is modified with a specific phase-shift φ_m and passes through the left aperture. The beam reflected by the fixed segment is unmodified, part of which passes through the right aperture. Then an image of the interference fringes is formed on the CCD camera with a exposure time of 100 microseconds, supposing the optical path difference (OPD) is shorter than the coherence length, which is easy to achieve for a narrow spectrum. The image also represents the point spread function (PSF) of the light source. After the position of the moving segment is changed and the beam with the given phase-shifts $\{0, \pi/2, \pi, 3\pi/2\}$ is modified, a group of PSFs can be obtained. Then the fractional phase error can be extracted from the PSFs using equation (3), (5) in Section 2. Via adjusting the tunable filter system and changing the spectrum, three phase measurements at three wavelengths can be obtained. Then the complete OPD can be resolved by combining the three measurements.

Also the scene can be changed to an extended object uniformly illuminated by a wide band light-emitting-diode (LED) with a diffuser inserted into its illumination path as shown in Fig. 3. A resolution test chart is chosen as the target to show an intuitive resolution improvement.

4. Experimental Results

In this section, the performance of the multi-spectral piston sensing technology was examined. Firstly, the method was applied to co-phasing the two-aperture imaging system, and the fruit was evaluated on both point target and extended target. Then a quantity of tests was carried out to compare the pistons obtained by our method with the known values generated by the phase-moving mirror, thus the accuracy and the capture range of the method were obtained.

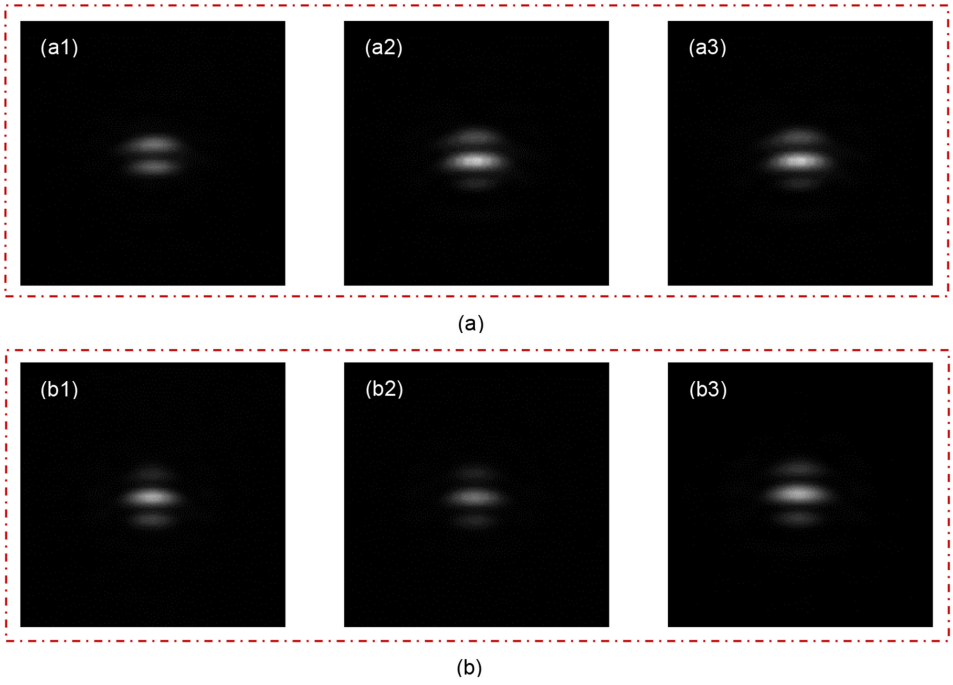

Fig. 5. Point source interferograms of the (a) uncorrected and (b) corrected two aperture system at the three wavelengths, with sub-captions being (a1), (a2), (a3) & (b1), (b2), (b3).

4.1 Cophasing Results

The phase-shift mirror divides the collimated beam into two paths and modulates one of them, thus specific phase shifts were added to the two-aperture imaging system. However, the phase-shift mirror itself also introduces piston error since the two segments of it naturally don't accurately lie in the same plane, and the piston error can hardly be eliminated manually due to the existence of "2π ambiguity". The multi-spectral piston sensing technology was used to measure the piston error introduced by the instrument. The adopted central wavelengths of the three narrow spectrums were 495 nm, 525 nm and 555 nm with bandwidths $>$14 nm (meaning that the coherent lengths of the three spectrums are shorter than 17.5 um, 19.6 um, 22 um, respectively). The performance of the corrected two-aperture imaging system was evaluated on both point target and extend target.

The results are shown in Figs. 5 and 6. Fig. 5(a1)–(a3) shows the point source interferograms of the two aperture imaging system in three wavelengths, i.e., 495 nm, 525 nm and 555 nm, respectively. By definition, the point source interferograms are point spread function graphs of the optical imaging system. The irregular distribution of the point spread functions indicates that the two aperture imaging system is affected by optical path differences (OPD). Thus the multi spectral piston sensing technology was applied to the two aperture system to correct the phase error. The point spread function graphs of the corrected system are shown in Fig. 5(b1)–(b3), respectively. The symmetrical three strip distributions of the point spread functions prove that the two aperture imaging system is cophased synchronously under three discrete wavelengths, since the three wavelengths are not multiples of each other, 2π ambiguity of the piston error is indicated to be elimated and the two aperture imaging system meets the main specification of co-phasing. Then the corrected two aperture system was applied to observe the extended target with a wide band light source. The bandwidth of the light source was 80 nm and the central wavelength was 535 nm. The images formed in the focus plane are shown in Fig. 6. In the images formed from the upper aperture and lower aperture individually, the 7th strips group of resolution test chart can hardly be distinguished. However, the horizontal stripes of the 23th strips group in the inner ring of the

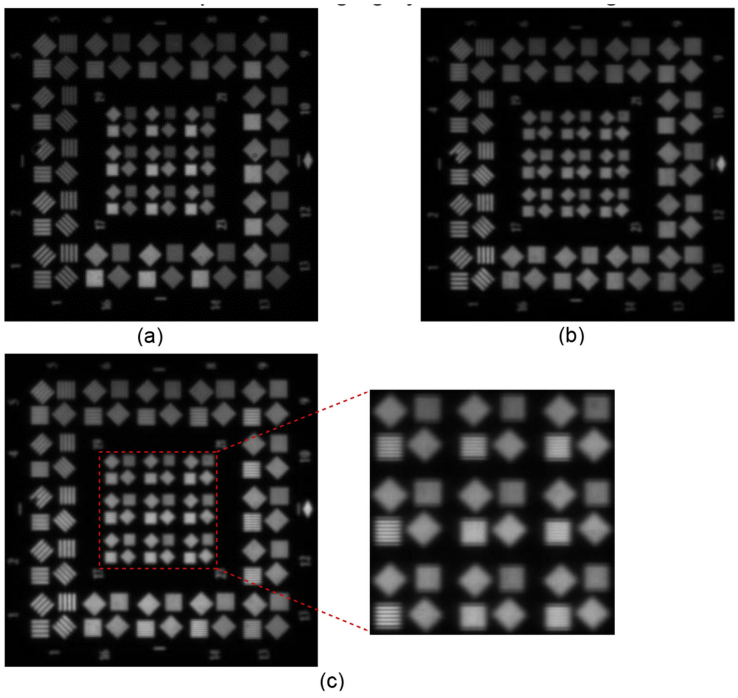

Fig. 6. Images of the resolution test chart. (a) image formed by the upper aperture; (b) image formed by the lower aperture; (c) image formed by the corrected two-aperture system.

resolution test chart can be figured out. The vertical resolution of the two aperture imaging system is much higher than of a single aperture system.

4.2 Cophasing Results Accuracy and Capture Range

A series of tests were conducted to compare the piston values resolved by our method with the artificially introduced piston errors. The initial piston errors and the measured piston errors are provided in Table 1.

Since interference fringes can be hardly captured with 495 nm central operation wavelength when we introduce piston errors larger than 8 um. We artificially introduce piston errors ranging roughly from -8 um to 8 um. The average peak signal-to-noise ratio (PSNR) of the captured interference images is about 36.4 dB. The results in Table 1 show that the measured piston errors agree well with the initial introduced piston errors. The difference between the initial pistons and the measured pistons represents the residual errors of the measurements. The average value of the residual errors is -0.003 um and the root mean square (RMS) value is 0.018 um.

Also, it is necessary to check the relative piston measuring results. In theory, there should be a series of relative piston errors among the artificially introduced piston errors shown in Table 1. Taking the first group of initial and measured piston error (-0.254 um, -0.253 um) in Table 1 as a reference, we can obtain a series of relative introduced piston and measured piston groups by an operation of subtraction between the first group (-0.254 um, -0.253 um) with other initial and measured piston groups. Fig. 7(a) shows that the profile of relative measured piston values agrees well with the profile of relative introduced piston errors. The difference between the initial pistons and the measured pistons is presented as the residual errors in Fig. 7(b). The average value of the residual errors is about -0.003 um and the root mean square (RMS) value is less than 0.017 um. In summary, the method successfully handled an amplitude of correction of ± 8 um, while the accuracy is 0.018 um.

TABLE 1
Initial, Measured and Difference Values of the Piston Errors

Piston (um)			Piston (um)			Piston (um)		
Initial	Measured	Difference	Initial	Measured	Difference	Initial	Measured	Difference
-0.254	-0.253	0.001	-4.112	-4.112	0	1.915	1.933	0.018
-0.527	-0.532	-0.005	-4.507	-4.53	-0.023	2.042	2.05	0.008
-0.717	-0.723	-0.005	-4.819	-4.813	0.006	2.757	2.799	0.042
-1.239	-1.252	-0.013	-5.988	-5.988	0	3.562	3.531	-0.031
-1.43	-1.45	-0.02	-6.814	-6.83	-0.016	4.945	4.952	0.007
-1.959	-1.983	-0.024	-7.135	-7.163	-0.028	5.659	5.661	0.002
-2.361	-2.373	-0.012	-7.87	-7.906	-0.036	6.338	6.362	0.024
-2.69	-2.685	0.005	0.064	0.06	-0.004	6.368	6.368	0
-3.08	-3.089	-0.009	0.516	0.518	0.002	7.069	7.087	0.018
-3.392	-3.405	-0.007	1.225	1.226	0.001	7.075	7.073	-0.002
-3.796	-3.8	-0.004	1.316	1.335	-0.019	7.78	7.815	0.035

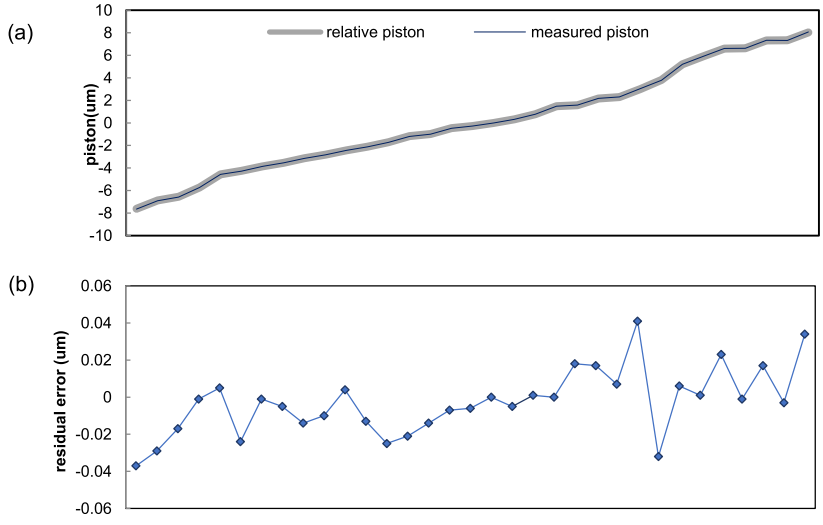

Fig. 7. Relative piston measuring results (a) initial and measured piston errors and (b) residual errors.

5. Conclusion

In this paper, the multi-spectral phase-shifting piston sensing technology has been experimentally demonstrated. The tests were performed in a simplified two-aperture imaging system. To conduct the tests, we have originally designed and implemented a phase-shifting mirror for the method. The phase shifting mirror can act as not only a phase shifter, but also a piston error generator and an aberration corrector in our experiments. The method was used to phase the two-aperture telescope with piston error up to ± 8 um, and the corrected two-aperture telescope performs well for both point target and extended target, indicating that the method perfectly meets the main specifications of co-phasing. What's more, since this technology provides fast and direct phase measurements by using simple numerical algorithms, it can be used in AO systems for real time correction. Predictably, the speed of this technology can be further improved by using a diffraction mirror to obtain modulated PSF images in several separate spectrums synchronously. The multi-spectral piston sensing technology may be widely used for co-phasing giant segmented mirrors and multi-aperture telescopes. Future work will focus on applying this method on an actual optical synthetic imaging system with the potential diffculties such as at low flux regime and short exposure time.

5. Acknowledgment

The authors would like to thank the anonymous reviewers for their valuable suggestions.

References

[1] H. Ma *et al.*, "Synthetic aperture imaging by using spatial modulation diversity technology with stochastic parallel gradient descent algorithm," *Opt. Exp.*, vol. 23, no. 11, pp. 14836–14849, 2015.
[2] Z. Xie *et al.*, "Restoration of sparse aperture images using spatial modulation diversity technology based on a binocular telescope testbed," *IEEE Photon. J.*, vol. 9, no. 3, Jun. 2017, Art. no. 7802611.
[3] E. Onillon *et al.*, "Mechanical slit mask mechanism breadboard for the MOSFIRE instrument of the KECK telescope spectrometer," in *Proc. Int. Conf. IEEE/ASME Adv. Intell. Mechatron.*, 2007, pp. 1–5.
[4] J. E. Nelson and P. R. Gillingham, "Overview of the performance of the W.M. Keck Observatory," in *Proc. SPIE, Adv. Technol. Opt. Telescopes V*, 1994, vol. 2199, pp. 82–93.
[5] GTC Website. [Online]. Available: http://www.gtc.iac.es/
[6] M. Clampin, "Status of the James Webb space telescope observatory," in *Proc. SPIE, Space Telescopes Instrum. Opt., Infrared, Millimeter Wave*, 2012, vol. 8442, Art. no. 84422A.
[7] J. Nelson and G. H. Sanders, "The status of the thirty meter telescope project," in *Proc. SPIE, Ground-Based Airborne Telescopes II*, 2008, vol. 7012, Art no. 70121.
[8] M. L. Louarn, P.-Y. Madec, E. Marchetti, H. Bonnet, and M. Esselborn, "Simulations of E-ELT telescope effects on AO system performance," in *Proc. SPIE Adaptive Opt. Syst. V*, 2016, vol. 9909, Art. no. 990975.
[9] J. M. Hill, "The large binocular telescope," *Appl. Opt.*, vol. 49, no. 16, pp. 115–122, 2010.
[10] S. J. Chung, D. W. Miller, and O. L. Weck, "ARGOS testbed: Study of multidisciplinary challenges of future spaceborne interferometric arrays," *Opt. Eng.*, vol. 43, no. 43, pp. 2156–2167, 2004.
[11] R. L. Kendrick *et al.*, "Wide-feld Fizeau imaging telescope: Experimental results," *Appl. Opt.*, vol. 45, no. 18, pp. 4235–4240, 2006.
[12] G. Chanan, C. Ohara, and M. Troy, "Phasing the mirror segments of the Keck telescopes II: The narrow-band phasing algorithm," *Appl. Opt.*, vol. 39, no. 25, pp. 4706–4714, 2000.
[13] G. Chanan, M. Troy, and E. Sirko, "Phase discontinuity sensing: A method for phasing segmented mirrors in the infrared," *Appl. Opt.*, vol. 38, no. 4, pp. 704–713, 1999.
[14] R. G. Paxman and J. R. Fienup, "Optical misalignment sensing and image reconstruction using phase diversity," *J. Opt. Soc. Amer. A.*, vol. 5, no. 5, pp. 914–923, 1988.
[15] A. Mazine and K. Heggarty, "Phase mapping and wavefront analysis based on multi-illumination light fields generated by a spatial light modulator," *Appl. Opt.*, vol. 50, no. 17, pp. 2679–2691, 2011.
[16] D. B. Moore and J. R. Fienup, "Subaperture translation estimation accuracy in transverse translation diversity phase retrieval," *Appl. Opt.*, vol. 55, no. 10, pp. 2526–2536, 2016.
[17] V. Borkowski *et al.*, "Sensitivity of a "dispersed-speckles" piston sensor for multi-aperture interferometers and hypertelescopes," *Astron. Asrophys.*, vol. 429, no. 2, pp. 747–753, 2005.
[18] F. Hénault, "Multi-spectral piston sensor for co-phasing giant segmented mirrors and multi-aperture interferometric arrays," *J. Opt. A, Pure Appl. Opt.*, vol. 11, no. 12, pp. 802–807, 2009.
[19] F. Hénault, "Conceptual design of a phase shifting telescope-interferometer," *Opt. Commun.*, vol. 261, no. 1, pp. 34–42, 2006.
[20] M. G. Lofdahl and H. Eriksson, "Resolving piston ambiguities when phasing a segmented mirror," in *Proc. SPIE, UV, Opt., IR Space Telescopes Instrum.*, 2000, vol. 4013, pp. 774–782.